Thin films in partial wetting: internal selection of contact-line dynamics

Amir Alizadeh Pahlavan, Luis Cueto-Felgueroso, Gareth H. McKinley, and Ruben Juanes*

Massachusetts Institute of Technology, 77 Massachusetts Avenue, Cambridge, Massachusetts 02139, USA

(Dated: May 7, 2015)

When a liquid touches a solid surface, it spreads to minimize the system's energy. The classic thin-film model describes the spreading as an interplay between gravity, capillarity and viscous forces, but cannot see an end to this process as it does not account for the non-hydrodynamic liquid–solid interactions. While these interactions are important only close to the contact line, where the liquid, solid and gas meet, they have macroscopic implications: in the partial-wetting regime, a liquid puddle ultimately stops spreading. We show that by incorporating these intermolecular interactions, the free energy of the system at equilibrium can be cast in a Cahn–Hilliard framework with a height-dependent interfacial tension. Using this free energy, we derive a mesoscopic thin-film model that describes statics and dynamics of liquid spreading in the partial-wetting regime. The height-dependence of the interfacial tension introduces a localized apparent slip in the contact-line region and leads to compactly-supported spreading states. In our model, the contact line dynamics emerge naturally as part of the solution and are therefore non-locally coupled to the bulk flow. Surprisingly, we find that even in the gravity-dominated regime, the dynamic contact angle follows the Cox–Voinov law.

Pour a glass of water on a table; what happens? It spreads for a while and stops. This process seems simple enough to be described by a reduced-order model, and indeed the classic thin-film model is a step in this direction [1]. This model can be derived from the Stokes equations using the lubrication approximation, but it contains no information about the interactions between the liquid and the underlying solid surface. While these interactions are of non-hydrodynamic origin and only become significant at heights less than $\sim 100\,\mathrm{nm}$ [2], they have pronounced macroscopic implications: the classic model, which does not incorporate these intermolecular interactions, predicts that the liquid never stops spreading, in stark contrast with the basic observation of a static puddle that forms in the partial-wetting regime.

A liquid is said to be partially wetting to a surface when it forms a contact angle in the range of $0 < \theta_Y \leq \pi/2$ at equilibrium. This equilibrium contact angle is well described by the Young equation, $\cos\theta_Y = (\gamma_{sg} - \gamma_{sl})/\gamma$, where γ_{sg}, γ_{sl} and γ are solid–gas, solid–liquid, and liquid–gas interfacial energies [3]. To extend the classical description to the partial-wetting regime, one can supplement it with non-hydrodynamic interactions as a boundary condition at the contact line [1, 4]. When capillary forces are the dominant driving mechanism, the dynamic contact angle, θ_d, has been shown to follow the Cox–Voinov law, $\theta_d^3 = \theta_Y^3 + 9\mathrm{Ca}\ln(l_M/l_\mu)$ [4–6], where $\mathrm{Ca} = \eta U/\gamma$ is the capillary number with liquid viscosity η and contact line velocity U; l_M and l_μ are characteristic macroscopic and microscopic length scales in the problem. Despite its success in matching experimental data, invoking this boundary condition does not address the question of how the non-hydrodynamic forces determine the emerging dynamics at the macroscopic scale.

Here, we work within the long-wave approximation to derive a generalized mesoscopic thin-film equation that captures the dynamics of the moving contact line self-consistently as part of the solution, making it non-locally coupled to the rest of the system. Within the framework of the non-equilibrium thermodynamics, a conservation equation for the height of the liquid film h can be written as [7]:

$$\frac{\partial h}{\partial t} = \nabla \cdot \left(\mathcal{M}(h) \nabla \left(\frac{\delta \Gamma}{\delta h} \right) \right), \tag{1}$$

where $\mathcal{M}(h)$ is the mobility, Γ is the free energy, and $\delta\Gamma/\delta h = \partial\Gamma/\partial h - \nabla \cdot [\partial\Gamma/\partial(\nabla h)]$ is the variational derivative of the free energy with respect to height. We start by deriving the free energy Γ of a non-volatile liquid puddle on a solid surface. At equilibrium, the variation of the free energy is zero, $\delta\Gamma = 0$. Writing the free energy as $\Gamma = \int \Phi(h, \nabla h)\, dX$ and using the calculus of variations, we arrive at the following two equations for the specific free energy Φ [8, 9]:

$$\frac{\partial \Phi}{\partial h} - \frac{\partial}{\partial h}\left(\frac{\partial \Phi}{\partial \nabla h} \right) = 0, \tag{2}$$

$$\left[\Phi - \nabla h \cdot \left(\frac{\partial \Phi}{\partial \nabla h} \right) \right]_{h=0} = 0, \tag{3}$$

known as the Euler–Lagrange and Augmented Young equations, respectively. Equation (2) determines the shape of the liquid surface at equilibrium and reduces to the Young–Laplace equation in the simplest form, while Eq. (3) serves as the boundary condition at the contact line.

Macroscopic contributions taken into account, we can write the free energy as $\Phi(h, \nabla h) \equiv \Phi_M(h, \nabla h) = 1/2\rho g h^2 + (\gamma_{sl} - \gamma_{sg}) + \gamma\sqrt{1 + (\nabla h)^2}$, in which ρ is the liquid density and g is the gravitational acceleration. The classic thin-film model can be recovered by putting the macroscopic free energy into the conservation Eq. (1). Substituting Φ_M into the Augmented Young equation, we recover the Young equation [3]. An often-overlooked constraint on the free energy is that as the height of the liquid film goes to zero, one should recover the solid–gas interfacial energy, $\lim_{h\to 0} \Phi = 0$ [3, 10]. It is straightforward to see that the only way to sat-

isfy this constraint with the macroscopic free energy is to have $\gamma + \gamma_{sl} = \gamma_{sg}$, corresponding to the complete-wetting regime.

Microscopic intermolecular forces close to the contact line must therefore be considered to arrive at a self-consistent description of the free energy for partial-wetting systems. These interactions are commonly known as surface forces [11] or disjoining/conjoining pressure [2]. Taking the intermolecular forces $\Phi_\mu(h)$ into account, we can write the free energy as $\Phi(h, \nabla h) \equiv \Phi_M(h, \nabla h) + \Phi_\mu(h)$. Substituting into the Augmented Young equation, we arrive at what is commonly known as the Derjaguin-Frumkin equation, $\cos\theta_Y = \cos\theta_\mu + \Phi_\mu(0)/\gamma$, relating the Young contact angle to the surface forces [8]. The Young angle is defined at the macro scale, whereas θ_μ is the microscopic contact angle [3, 8, 12], which needs to be zero for the free energy to be continuous. The combination of a non-zero Young contact angle and a zero microscopic contact angle indicates the existence of an ultra-thin liquid film around the main drop, the so-called pseudo-partial-wetting regime [10, 13]. While precursor films are commonly observed in the complete-wetting regime [14], they are not in non-volatile partial-wetting liquids [6, 10, 13]. We therefore need a description of the system's free energy that allows for non-zero microscopic contact angles.

Traditionally, surface forces are expressed as a function of film height only, since they are derived for parallel liquid–solid interfaces [1, 2]. Close to the contact line, however, the liquid and solid interfaces are not parallel and one should account for the interface slope to arrive at a proper description of the intermolecular forces [15, 16]. The free energy should therefore be written as $\Phi(h, \nabla h) \equiv \Phi_M(h, \nabla h) + \Phi_\mu(h, \nabla h)$. Consistent with the derivations of [16] and using the long-wave approximation, we propose to decompose the surface forces as $\Phi_\mu(h, \nabla h) = \phi_{\mu,1}(h) + \phi_{\mu,2}(h)(\nabla h)^2/2$. Substituting the free energy, Φ, into the Augmented Young equation and requiring the continuity of the free energy, it is straightforward to show that all constraints are satisfied without imposing any *a priori* condition on θ_μ if $\phi_{\mu,1}(0) = \mathcal{S}$ and $\phi_{\mu,2}(0) = -\gamma$, where $\mathcal{S} = \gamma_{sg} - \gamma_{sl} - \gamma$ is the spreading coefficient [10]. The microscopic contact angle therefore emerges naturally as part of the solution, consistent with the predictions of nonlocal density functional theory [17]. We can therefore write the free energy as:

$$\Gamma = \int \left[f(h) + \kappa(h)\frac{(\nabla h)^2}{2} \right] dX. \tag{4}$$

This free energy expression resembles the Cahn–Hilliard formulation [18], in which the free energy can be decomposed into bulk $f(h) = \rho g h^2/2 - \mathcal{S} + \phi_{\mu,1}(h)$ and interfacial $\kappa(h)(\nabla h)^2/2$ contributions, where $\kappa(h) = \gamma + \phi_{\mu,2}(h)$ can be interpreted as a height-dependent interfacial tension. A nonlinear KPZ-type term can be generated using this free energy [19]. The constraints on $\phi_{\mu,1}(0)$ and $\phi_{\mu,2}(0)$ imply that $f(0) = 0$ and $\kappa(0) = 0$. Vanishing of the interfacial tension as the film height tends to zero is required to arrive at compactly-supported spreading states [20], and our derived
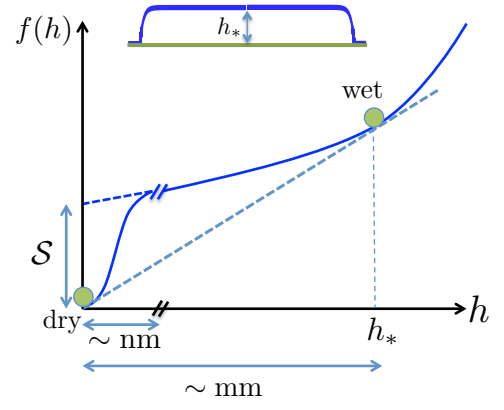

FIG. 1. Schematic of the tangent construction on the bulk free energy, $f(h)$, leading to the coexistence of wet, $h = h_*$, and dry, $h = 0$, states. In the absence of intermolecular forces, the bulk free energy can be written as $f(h) = \rho g h^2/2 - \mathcal{S}$, which does not reduce to the solid–gas interfacial energy as $h \to 0$ unless $\mathcal{S} = 0$, which implies complete wetting [10].

form of the free energy naturally meets this requirement. Another constraint on $\phi_{\mu,1}(h)$ can be incorporated through a tangent construction on the bulk free energy, which ensures that the two coexisting phases at equilibrium have the same chemical potential [21], i.e. $df/dh|_{h=0} = df/dh|_{h=h_*} = \rho g h_*$ (Fig. 1), where $h_* = 2\,l_\gamma \sin(\theta_Y/2)$ is the height of the liquid puddle that is set by a balance between gravity and surface tension, and $l_\gamma = \sqrt{\gamma/\rho g}$ is the capillary length [10]. To describe the functional form of $\phi_\mu(h)$, we use a surface force that consists of long-ranged attractive van der Waals forces and short-ranged repulsive forces, similar to an integrated Lennard-Jones potential [2]. Other combinations, such as long-ranged repulsive and short-ranged attractive interactions [22, 23] can also be used. We therefore write $\phi_{\mu,i}(h) = \alpha_i \left[(1+\beta_i)d_0^2/(h+d_0)^2 - \beta_i d_0^8/(h+d_0)^8 \right]$, where $d_0 = \sqrt{\mathcal{A}/6\pi\gamma} \approx 0.2\,\mathrm{nm}$ is a molecular length scale with $\mathcal{A}$ being the Hamaker constant [2, 10]. The coefficients $\alpha_1 = \mathcal{S}$, $\beta_1 = (1 - d_0/h_*)/3$ and $\alpha_2 = -\gamma$, $\beta_2 = 1/3$ are determined through imposing the constraints on $\phi_{\mu,i}(0)$, the tangent construction, and requiring the slope at the contact line to be non-zero. The denominator has been regularized by adding d_0, allowing us to recover the solid–liquid interfacial energy when the film height is zero [10, 16, 22].

Substituting the derived free energy from Eq. (4) back into the conservation Eq. (1) and nondimensionalizing the parameters as $\tilde{h} = h/h_*$, $\tilde{x} = x/R_f$, $\tilde{t} = t/(3\mu R_f^2/\rho g h_*^3)$, $\tilde{f} = f/\rho g h_*^2$, $\tilde{\kappa} = \kappa/\gamma$ and dropping the tilde for convenience, the generalized thin film equation takes the form:

$$\frac{\partial h}{\partial t} = \nabla \cdot \left\{ \mathcal{M}(h)\nabla \left[\frac{\partial f}{\partial h} - \frac{1}{\mathrm{Bo}}\sqrt{\kappa(h)}\nabla \cdot \left(\sqrt{\kappa(h)}\nabla h \right) \right] \right\}, \tag{5}$$

in which $\mathrm{Bo} = R_f^2/l_\gamma^2$ is the Bond number, where R_f is the characteristic lateral length of the liquid, taken to be its final equilibrium radius. We can approximate the volume of a liq-
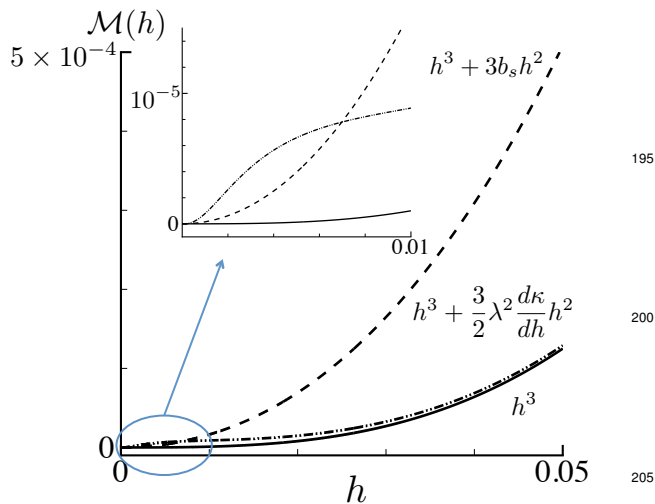
FIG. 2. Comparison of the mobility with and without slip ($\mathcal{M}(h) = h^3$ ——— , $\mathcal{M}(h) = h^3 + 3b_s h^2$, $b_s = 10d_0$ ---- , $\mathcal{M}(h) = h^3 + (3/2)\lambda^2(d\kappa/dh)h^2$, $\lambda = 10d_0$, $\theta_Y = \pi/12$ —··—). While Navier slip is global, our proposed slip model is localized to the contact-line region, where it dominates the Navier slip, consistent with molecular simulations [24, 25].

uid puddle as $V \approx \pi R_f^2 h_*$, whereas for small drops the final radius can be related to the volume using the spherical cap approximation. Vanishing of the interfacial tension $\kappa(h)$ at the contact line indicates that the order of the equation is reduced by one, pointing to a singular perturbation problem. This picture is consistent with the description suggested by de Gennes [26], indicating the dominance of intermolecular forces very close to the contact line, leading to a natural cut-off scale that removes the moving-contact-line singularity.

Starting from the Stokes equation, using the lubrication approximation, and assuming no slip at the wall and zero shear stress at the liquid–gas interface, $\tau = 0$ (neglecting the viscosity of the gaseous phase), the mobility in Eq. (1) is easily derived to be $\mathcal{M}(h) = h^3$. The no-slip boundary condition, however, will lead to the moving-contact-line singularity [28]. To resolve the singularity, the Navier slip boundary condition is generally used, introducing a slip velocity proportional to the shear stress in the liquid adjacent to the wall, $u_s = b_s \nabla u$ [29], where b_s is the slip length, which depends on the liquid–solid interaction [30]. The slip condition leads to a mobility of the form $\mathcal{M}(h) = h^3 + 3\,b_s h^2$. In immiscible flows however, slip has been shown to be localized to the contact-line region [24, 25] and to match the observations of molecular simulations, *ad hoc* functions with decaying slip away from contact line have been proposed [31].

The free energy derived in Eq. (4) incorporates a height-dependent interfacial tension $\kappa(h)$. A gradient in the interfacial tension leads to the Marangoni effect [32], which causes a non-zero shear stress at the liquid–gas interface, driving a net flow. In analogy with this effect, the height dependence of the interfacial tension leads to a non-zero interfacial shear stress at the liquid–gas interface, $\tau + \lambda^2(J \cdot t)d\kappa/dh = 0$,

where $J = \nabla(\delta\Gamma/\delta h)$ is proportional to the flux, t is the unit vector tangent to the interface and λ is an effective slip length. The variation of the interfacial tension is limited to the contact line region where intermolecular forces dominate. Away from the contact line ($d\kappa/dh = 0$) or at equilibrium ($J = 0$), the balance reduces to the usual zero shear stress at the liquid–gas interface ($\tau = 0$). Only during spreading does this non-zero interfacial stress come into play, hence the name "flow-induced Marangoni effect" [33]. Incorporating both this shear stress at the liquid–gas interface and the Navier slip boundary condition at the liquid–solid interface, we can write the mobility in the most general form as $\mathcal{M}(h) = h^3 + 3\left[b_s + (\lambda^2/2)d\kappa/dh\right]h^2 + 3b_s\lambda h$. This model bears similarities with the generalized Navier boundary condition [25], and slip due to the gradient of chemical potential close to the contact line [34]. Our proposed model therefore addresses two main requirements regarding slip at the contact line: 1) it is localized to the contact line region, and 2) it depends on the non-hydrodynamic interactions close to the contact line and introduces an energy scale [6] (Fig. 2).

We solve Eq. (5) using standard finite differences [35] and adaptive mesh refinement. The disparate length scales involved in this problem make the numerical computations prohibitively expensive. Since we are mainly interested in the macroscopic predictions of our model, we regularize the microscopic length d_0 by multiplying it by a magnifying factor 10^4, therefore bringing the peak of the energy function shown in Fig. 1 from the nano to the micro scale. For simplicity, we set the Navier slip length to zero, $b_s = 0$, and consider only the localized effective slip in the contact-line region, $\lambda = 10d_0$ (Fig. 2). We take the capillary length to be $l_\gamma = 1.5$mm, which is typical of silicone oil.
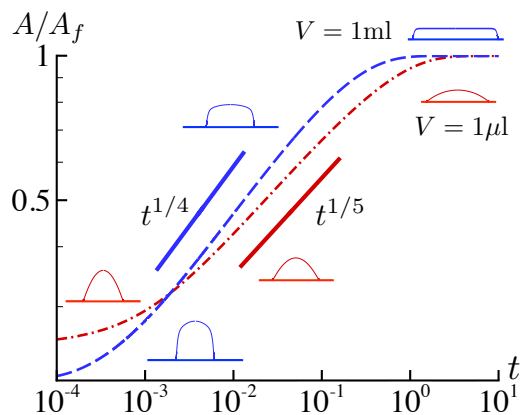
We now address the original question of how a liquid pud-

FIG. 3. The rate of spreading is influenced by the volume of liquid. For small volumes (Bo $\lesssim 1$, —·—), capillary forces are the dominant driving force and the drop takes the shape of a spherical cap while viscosity resists the spreading, leading to $A \sim t^{1/5}$. For large volumes (Bo ≈ 360, ----), gravity dominates capillary forces everywhere except very close to the moving contact line, leading to a $t^{1/4}$ scaling; the liquid puddle takes the shape of a pancake at equilibrium. A_f is the final equilibrium area and $\theta_Y = \pi/12$.
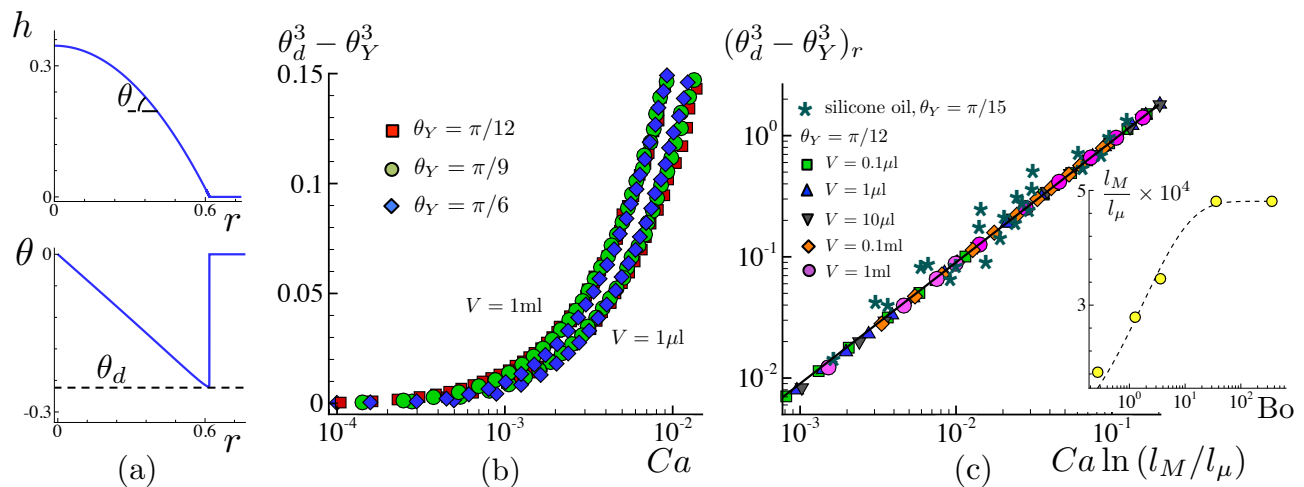
FIG. 4. (a) The dynamic contact angle is defined at the inflection point of the drop profile (top), where its slope (bottom) reaches a plateau ($\tan\theta = (h_*/R_f)(dh/dr)$). (b) The dynamic contact angle, θ_d, follows the Cox–Voinov law $\theta_d^3 - \theta_Y^3 = 9\mathrm{Ca}\ln(l_M/l_\mu)$, but increases with the volume of the liquid. (c) The nonlocal influence of bulk flow can be conflated into the macroscopic length scale, l_M, leading to a collapse of the dynamic contact angle data for the different volumes onto a single curve (solid line represents the Cox–Voinov law). The stars represent the classic experiments of [27] corresponding to the silicone oil-air interface in a capillary tube ($l_M/l_\mu \approx 1.25 \times 10^3$). The rescaled contact angle data from the model accounts for the fact that the microscopic length scale l_μ is magnified by 10^4 in the simulations: $(\theta_d^3 - \theta_Y^3)_r = \theta_d^3 - \theta_Y^3 + (9\ln 10^4)\mathrm{Ca}$, (inset: an approximate fit $l_M/l_\mu = 4.8(1 - exp(-0.75\mathrm{Bo}^{1/2}))$ is shown as the dashed line)

dle spreads on a solid surface. We expect a partial-wetting liquid to spread initially to minimize the system's free energy and to stop spreading when it reaches equilibrium. For small liquid volumes, i.e. when Bo $\lesssim$ 1, capillarity is the dominant driving force while viscosity resists the spreading. A simple scaling between these two dominant forces leads to Tanner's law for spreading, which predicts that the wetted area, $A(t)$, scale as $t^{1/5}$ [36] (Fig. 3). In this regime, the liquid drop takes the shape of a spherical cap that spreads quasi-statically. As the volume of the liquid increases, i.e. Bo $\gg$ 1, gravity becomes the dominant driving force in the bulk while surface tension effects remain limited to the vicinity of the moving contact line [37–39]. Balancing the gravity and viscous forces acting at the macroscopic scale, one arrives at a scaling of $t^{1/4}$ for the wetted area. In this regime, the spherical-cap approximation is no longer valid, but similarity solutions for the quasi-static spreading can still be obtained [38, 39]. In both the capillary and gravity-dominated regimes, the final approach to equilibrium is exponential [39, 40], deviating markedly from the quasi-static self-similar power-law behavior. Our model predicts this final approach to a compactly-supported spreading state (Fig. 3).

While the macroscopic spreading rate is a good measure for examining the validity of our model, it is not very sensitive to the contact line dynamics, which arrest the spreading drop as it approaches equilibrium. A correct description of the contact line dynamics is therefore needed to properly describe this final stage. In the capillary-dominated regime, the Cox–Voinov law describes the dependence of the dynamic contact line on the spreading rate [4–6]. Our model indeed displays excellent agreement with the Cox–Voinov law for different equilibrium contact angles θ_Y [Fig. 4(b)]. Consistent with

earlier observations [41], the dynamic contact angle exhibits a dependence on the liquid volume. This dependence is expected, as the macroscopic length l_M in the Cox–Voinov law is related to the radius of the drop [4, 42], which scales with its volume ($R_f \sim V^{1/3}$ in the capillary-dominated regime and $R_f \sim (V/h_*)^{1/2}$ in the gravity-dominated regime). The surprising observation, however, is that the Cox–Voinov law provides an excellent description of the dynamic contact angle even in the gravity-dominated regime. This observation is supported by early experiments in the complete-wetting regime [43]. The macroscopic length scale, l_M, increases with volume and thus with the Bond number, but saturates to a constant value (proportional to the capillary length) beyond the transition from capillary-dominated to gravity-dominated regime (at Bo $\approx$ 30). Taking the effective slip length to be the microscopic length scale $l_\mu = \lambda$, we find the macroscopic length scale l_M by fitting the dynamic contact angle data to the Cox–Voinov law ($l_M \approx 100\,\mu$m in the gravity-dominated regime). Taking the dependence of the macroscopic length scale on the volume into account, we observe a remarkable collapse of all the dynamic contact angle data corresponding to different volumes onto a single curve [Fig. 4(c)].

In summary, we have shown that incorporating non-hydrodynamic interactions between the liquid and solid in a self-consistent manner leads to a free energy that can be cast in a Cahn–Hilliard formulation with a height-dependent interfacial tension. This height-dependence allows compactly-supported spreading states with no precursor film [20], in contrast with the classic thin-film model that does not admit such solutions [44]. The height-dependence of the interfacial tension further introduces an effective slip that is localized to the contact-line region, where it dominates the Navier

slip, consistent with the observations of molecular simulations [24, 25]. Our thin-film model predicts that the dynamic contact angle follows the Cox–Voinov law both in the capillary-dominated and gravity-dominated regimes. This feature illustrates the ability of our mesoscopic model to capture nonlocal effects on the contact line dynamics, which exert a fundamental control on pattern formation in immiscible porous media flows [45].

* juanes@mit.edu

[1] A. Oron, S. H. Davis, and S. G. Bankoff, Rev. Mod. Phys. **69**, 931 (1997); R. V. Craster and O. K. Matar, *ibid*. **81**, 1131 (2009).

[2] J. N. Israelachvili, *Intermolecular and Surface Forces: Third ed.* (Academic Press, 2011).

[3] P. G. de Gennes, Rev. Mod. Phys. **57**, 827 (1985).

[4] D. Bonn, J. Eggers, J. Indekeu, J. Meunier, and E. Rolley, Rev. Mod. Phys. **81**, 739 (2009).

[5] O. Voinov, Fluid Dyn. **11**, 714 (1976); R. G. Cox, J. Fluid Mech. **168**, 169 (1986).

[6] J. H. Snoeijer and B. Andreotti, Annu. Rev. Fluid Mech. **45**, 269 (2013).

[7] P. C. Hohenberg and B. I. Halperin, Rev. Mod. Phys. **49**, 435 (1977); J. W. Cahn, Acta Metall. **9**, 795 (1961); V. S. Mitlin, J. Colloid Interface Sci. **156**, 491 (1993).

[8] E. K. Yeh, J. Newman, and C. J. Radke, Colloid Surf. A **156**, 137 (1999); V. M. Starov, M. G. Velarde, and C. J. Radke, *Wetting and Spreading Dynamics* (CRC press, 2007).

[9] M. D. Greenberg, *Foundations of Applied Mathematics* (Courier Corporation, 1978).

[10] P.-G. de Gennes, F. Brochard-Wyart, and D. Quéré, *Capillarity and Wetting Phenomena: Drops, Bubbles, Pearls, Waves* (Springer, 2004).

[11] B. Derjaguin, N. Churaev, and V. Muller, *Surface Forces* (Springer, 1987).

[12] T. Pompe and S. Herminghaus, Phys. Rev. Lett. **85**, 1930 (2000).

[13] F. Brochard-Wyart, J. M. Di Meglio, D. Quéré, and P. G. De Gennes, Langmuir **7**, 335 (1991); G. Reiter, A. Sharma, A. Casoli, M.-O. David, R. Khanna, and P. Auroy, *ibid*. **15**, 2551 (1999).

[14] H. P. Kavehpour, B. Ovryn, and G. H. McKinley, Phys. Rev. Lett. **91**, 196104 (2003); A. Hoang and H. P. Kavehpour, *ibid*. **106**, 254501 (2011); M. N. Popescu, G. Oshanin, S. Dietrich, and A.-M. Cazabat, J. Phys. Condens. Matter **24**, 243102 (2012).

[15] C. Miller and E. Ruckenstein, J. Colloid Interface Sci. **48**, 368 (1974); L. M. Hocking, Phys. Fluids A-Fluid **5**, 793 (1993); S. Kalliadasis and H.-C. Chang, Ind. Eng. Chem. **35**, 2860 (1996); Q. Wu and H. Wong, J. Fluid Mech. **506**, 157 (2004).

[16] B. Dai, L. G. Leal, and A. Redondo, Phys. Rev. E **78**, 061602 (2008).

[17] J. H. Snoeijer and B. Andreotti, Phys. Fluids **20**, 057101 (2008).

[18] J. W. Cahn and J. E. Hilliard, J. Chem. Phys. **28**, 258 (1958).

[19] M. Kardar, G. Parisi, and Y.-C. Zhang, Phys. Rev. Lett. **56**, 889 (1986); M. Kardar, *Statistical Physics of Fields* (Cambridge University Press, 2007).

[20] R. Benzi, M. Sbragaglia, M. Bernaschi, and S. Succi, Phys. Rev. Lett. **106**, 164501 (2011); L. Cueto-Felgueroso and R. Juanes, *ibid*. **108**, 144502 (2012).

[21] J. S. Rowlinson and B. Widom, *Molecular Theory of Capillarity* (Courier Corporation, 1982); A. J. Bray, Adv. Phys. **51**, 481 (2002).

[22] A. Sharma, Langmuir **9**, 861 (1993); **9**, 3580 (1993).

[23] L. M. Pismen and Y. Pomeau, Phys. Rev. E **62**, 2480 (2000); U. Thiele, M. G. Velarde, and K. Neuffer, Phys. Rev. Lett. **87**, 016104 (2001).

[24] J. Koplik, J. R. Banavar, and J. F. Willemsen, Phys. Rev. Lett. **60**, 1282 (1988); P. A. Thompson and M. O. Robbins, **63**, 766 (1989); J. B. Freund, Phys. Fluids **15**, L33 (2003).

[25] T. Qian, X.-P. Wang, and P. Sheng, Phys. Rev. E **68**, 016306 (2003); Phys. Rev. Lett. **93**, 094501 (2004); J. Fluid Mech. **564**, 333 (2006); W. Ren and W. E, Phys. Fluids **19**, 022101 (2007); W. Ren, D. Hu, and W. E, **22**, 102103 (2010).

[26] P. G. D. Gennes, X. Hua, and P. Levinson, J. Fluid Mech. **212**, 55 (1990).

[27] R. L. Hoffman, J. Colloid Interface Sci. **50**, 228 (1975); M. Fermigier and P. Jenffer, **146**, 226 (1991).

[28] C. Huh and L. Scriven, J. Colloid Interface Sci. **35**, 85 (1971); E. B. Dussan V. and S. H. Davis, J. Fluid Mech. **65**, 71 (1974).

[29] C. Neto, D. R. Evans, E. Bonaccurso, H.-J. Butt, and V. S. J. Craig, Rep. Prog. Phys. **68**, 2859 (2005); E. Lauga, M. Brenner, and H. Stone, in *Springer Handbook of Experimental Fluid Mechanics* (Springer, 2007) pp. 1219–1240.

[30] D. M. Huang, C. Sendner, D. Horinek, R. R. Netz, and L. Bocquet, Phys. Rev. Lett. **101**, 226101 (2008); L. Bocquet and E. Charlaix, Chem. Soc. Rev. **39**, 1073 (2010).

[31] E. B. Dussan V., J. Fluid Mech. **77**, 665 (1976); M.-Y. Zhou and P. Sheng, Phys. Rev. Lett. **64**, 882 (1990); N. G. Hadjiconstantinou, Phys. Rev. E **59**, 2475 (1999).

[32] V. G. Levich and V. S. Krylov, Annu. Rev. Fluid Mech. **1**, 293 (1969).

[33] Y. D. Shikhmurzaev, J. Fluid Mech. **334**, 211 (1997); *Capillary Flows with Forming Interfaces* (CRC Press, 2007); D. N. Sibley, N. Savva, and S. Kalliadasis, Phys. Fluids **24**, 082105 (2012).

[34] E. Ruckenstein and C. Dunn, J. Colloid Interface Sci. **59**, 135 (1977); L. M. Pismen and B. Y. Rubinstein, Langmuir **17**, 5265 (2001).

[35] J. A. Diez, L. Kondic, and A. Bertozzi, Phys. Rev. E **63**, 011208 (2000).

[36] L. H. Tanner, J. Phys. D: Appl. Phys. **12**, 1473 (1979).

[37] J. Lopez, C. A. Miller, and E. Ruckenstein, J. Colloid Interface Sci. **56**, 460 (1976).

[38] H. E. Huppert, J. Fluid Mech. **121**, 43 (1982).

[39] L. M. Hocking, Q. J. Mech. Appl. Math. **36**, 55 (1983).

[40] M. J. de Ruijter, J. De Coninck, and G. Oshanin, Langmuir **15**, 2209 (1999).

[41] J.-D. Chen, J. Colloid Interface Sci. **122**, 60 (1988); S. N. Reznik and A. L. Yarin, Phys. Fluids **14**, 118 (2002).

[42] J. Eggers and H. A. Stone, J. Fluid Mech. **505**, 309 (2004).

[43] C. Redon, F. Brochard-Wyart, H. Hervet, and F. Rondelez, J. Colloid Interface Sci. **149**, 580 (1992).

[44] M. Brenner and A. Bertozzi, Phys. Rev. Lett. **71**, 593 (1993).

[45] N. Martys, M. Cieplak, and M. O. Robbins, Phys. Rev. Lett. **66**, 1058 (1991); D. Geromichalos, F. Mugele, and S. Herminghaus, **89**, 104503 (2002); L. Cueto-Felgueroso and R. Juanes, **101**, 244504 (2008).